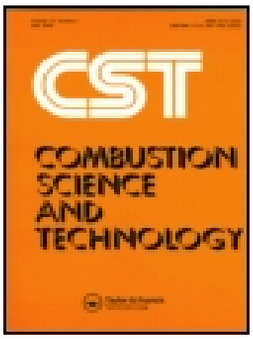

Taylor & Francis
Taylor & Francis Group

Combustion Science and Technology

ISSN: (Print) (Online) Journal homepage: https://www.tandfonline.com/loi/gcst20

Density Functional Theory Study on the Reduction of NO by CO Over Fe_3O_4 (111) Surface

Lilin Hu, Yang Zhang, Qing Liu & Hai Zhang

To cite this article: Lilin Hu, Yang Zhang, Qing Liu & Hai Zhang (2022): Density Functional Theory Study on the Reduction of NO by CO Over Fe_3O_4 (111) Surface, Combustion Science and Technology, DOI: 10.1080/00102202.2022.2130282

To link to this article: https://doi.org/10.1080/00102202.2022.2130282

Published online: 02 Oct 2022.

COMBUSTION SCIENCE AND TECHNOLOGY
https://doi.org/10.1080/00102202.2022.2130282

Density Functional Theory Study on the Reduction of NO by CO Over Fe_3O_4 (111) Surface

Lilin Hu, Yang Zhang, Qing Liu, and Hai Zhang

Key Laboratory for Thermal Science and Power Engineering of Ministry Education, Department of Energy and Power Engineering, Tsinghua University, Beijing, China

ABSTRACT

Iron or its oxides (Fe_xO_y) commonly exist in the ash of fossil fuel and biomass, and are used as oxygen carriers in chemical looping process, and Fe_3O_4 is a main occurrence. The NO reduction mechanisms by CO over Fe_3O_4 (111) surface was investigated via density functional theory (DFT) calculations. An optimized unit cell of Fe_3O_4 was constructed. The interaction between molecules and cell surface was described by the calculated adsorption properties and electronic structures. Results showed that the most stable adsorption of NO/CO belongs to chemisorption and NO has higher adsorption energy than CO. NO can be absorbed onto Fe_3O_4 surface to form $(NO)_2$ dimer structure, which easily decomposes via a small energy barrier. $(NO)_2$ dimer mechanism is a possible pathway for the reduction of NO by CO over Fe_3O_4, following three steps: $2NO \rightarrow (NO)_2^*$, $(NO)_2^* \rightarrow N_2O + O^*$, $O^* + CO^* \rightarrow CO_2$. After the decomposition, the intermediate species N_2O molecule and the remaining O atom adsorbed strongly on the Fe_3O_4 surface can be removed by CO. CO also promotes the gaseous decomposition of N_2O. DFT results also showed O_2 will prevent NO reduction reaction. The calculated reaction rate constants further verify the existence of $(NO)_2$ dimer mechanism and the rate-limiting step is the removal of the surface O atom.

ARTICLE HISTORY
Received 27 June 2022
Accepted 22 September 2022

KEYWORDS
Fe_3O_4; NO reduction; catalytic effect; DFT calculation

Introduction

NOx is one of the main pollutants generated by fuel combustion. To strictly control the NOx emission, selective catalytic reduction (SCR) or selective non-catalytic reduction (SNCR) techniques are often used for flue gas treatment (Yue et al. 2020). Though working effectively, both techniques use ammonia or urea as reducing agents. These agents are feedstocks of agricultural fertilizer and other chemicals, and their transport and storage need special care, especially for those near-city power plants. In addition, the over-use of reducing agent or poor mixing between reducing agent and flue gas can often cause NH_3-slip and aggravate ash deposition on the air preheater (Cheng et al. 2018). Moreover, for SCR, precious and hazardous metals such as vanadium and tungsten are used as the catalyst (Qin et al. 2016). Therefore, CO-SCR technology, which uses CO instead of NH_3 as reductant, was proposed (Boningari et al. 2018).

Iron element is an abundant element on the earth, and iron oxides are main constituents in the ash of coal, biomass, and some other solid fuels. In a combustion zone, CO is often

CONTACT Hai Zhang haizhang@tsinghua.edu.cn Key Laboratory for Thermal Science and Power Engineering of Ministry Education, Department of Energy and Power Engineering, Tsinghua University, Beijing 100084, China

rich. Given iron oxides behave as catalyst in NO reduction, they could be used for cost-effective CO-SCR technology development. Thus, it is significant to understand the effect of iron or its oxides on NOx reduction with the presence of CO.

In the past, many researches have conducted on the interaction of CO with iron or its oxides (Fe_xO_y) in iron making or chemical looping process, where Fe_2O_3 is a raw material or oxygen carrier. It was found Fe_2O_3 can be reduced by CO into different states (Chen et al. 2017; Monazam, Breault, and Siriwardane 2014; Prabakaran and Jayanti 2019; Wang et al. 2017), following a sequential order of $Fe_2O_3 \rightarrow FeO \rightarrow Fe$ (Chen et al. 2017) or $Fe_2O_3 \rightarrow Fe_3O_4 \rightarrow FeO$ (Monazam, Breault, and Siriwardane 2014), or parallel steps of $Fe_2O_3 \rightarrow Fe_3O_4$, $Fe_3O_4 \rightarrow FeO$ and $FeO \rightarrow Fe$ (Prabakaran and Jayanti 2019). During these processes, the conversion of $Fe_2O_3 \rightarrow Fe_3O_4$ takes place fast and completely (Prabakaran and Jayanti 2019; Wang et al. 2017). The processes of $Fe_3O_4 \rightarrow FeO$ and $FeO \rightarrow Fe$ are reversible. Therefore, iron may exist as Fe_3O_4 when CO is present. This is confirmed by the finding that the dominant iron oxide in ashes of coal-fired circulating fluidized bed boilers is Fe_3O_4 instead of Fe_2O_3 (Hou et al. 2008).

The effect of Fe_xO_y on NO reduction has been assessed. Hayhurst et al. (Hayhurst and Lawrence 1997; Hayhurst and Ninomiyas 1998) found that Fe has a strong catalytic effect on NO and N_2O reduction in a fluidized bed condition in a reducing atmosphere. The research of Zhou et al. (Zhou, et al. 2001) showed that the effect of Fe_2O_3/Fe_3O_4 on direct reduction of NO/N_2O is rather weak and CO can promote the reduction of N_2O. Xu et al. (Xu et al. 1999) and Li et al. (Li et al. 2016) also found Fe_2O_3 has remarkable catalytic effect on NO reduction in the presence of CO. However, the reaction mechanisms of NO and CO over Fe_3O_4 are still not clear.

Limited by the precision of measure methods, it is difficult to observe the reaction intermediates and therefore determine the reaction mechanism via experiments. Thus, molecular modeling methods have been developed to make up for this deficiency. Among them, density functional theory (DFT) calculation is an effective method to explore the microscopic reaction mechanism over catalysts surfaces at molecular level, via calculating the electronic structure of multi-electron systems (Sholl and Steckel 2009). The modeling uses distribution and rearrangement of electrons to reflect the formation or breakage of bonds and the interaction between molecules and a surface. DFT calculations have been used to investigate the adsorption of small molecules on the surface of iron oxides (Busch et al. 2018; Zhou et al. 2018) or the reduction mechanism of NO/N_2O on surface of different catalysts (Esrafili 2018; Hu et al. 2020; Wang, Zou, and Zhang 2022), and the calculation results of the adsorption of NO on Fe_3O_4 (111) agreed with experimental measurements (Busch et al. 2018). Some DFT calculations were also performed on the interaction of CO with pure and defective Fe_3O_4 (001) surfaces, but in absence of NO (Xue et al. 2014). Regarding to the reaction mechanisms of NO and CO over catalysts, DFT studies found that possible reactions involved with the formation of $(NO)_2^*$, N_2O, N_2 and O^* intermediates might exist and the rate determining steps differ from different catalysts (Esrafili 2018; Hu et al. 2020; Yan et al. 2021). Esrafili et al. verified the existence of $(NO)_2^*$ and O^* species on Si-BNNS catalyst. Hu et al. found that the rate determining step of $(NO)_2$ dimer mechanism on Fe-doped penta-graphene is the dissociation of $(NO)_2^*$. However, the reaction mechanisms of NO and CO over Fe_3O_4 and the intermediates are remained to be revealed.

Consequently, in this study, the reaction mechanisms of NO and CO over Fe_3O_4 were assessed using DFT modeling, via the embedded DMol3 module in Materials Studio (MS).

An optimized unit cell of Fe_3O_4 was constructed. The interaction between molecules and cell surface was described by the calculated adsorption properties and electronic structures. The reaction rates were calculated and possible reaction pathway is revealed.

Computational methods

Model of Fe_3O_4 (111)

A unit cell of Fe_3O_4 consisting of 24 Fe atoms and 32 O atoms has a cubic inverse spinel structure. Its optimized lattice constants ($a = b = c = 8.439$ Å, $\alpha = \beta = \gamma = 90°$) are consistent with the reported experimental data ($a = b = c = 8.390$ Å, $\alpha = \beta = \gamma = 90°$) (Wright, Attfield, and Radaelli 2002). Fe_3O_4 possesses two kinds Fe sites, that is, tetrahedral (8 Fe^{3+} ions, denoted as Fe_{Tet}) and octahedral sites (8 Fe^{3+} ions and 8 Fe^{2+} ions, denoted as Fe_{Oct}), manifesting different spin directions. In our calculation, the initial spin directions of tetrahedral and octahedral Fe sites were set as downward and upward, respectively and the total spin was allowed to be optimized. The calculated magnetic moment per Fe_3O_4 unit of 4.0 μB agreed well with experimental results. For the predominant natural growth faces of Fe_3O_4 (111) and Fe_3O_4 (001), Fe_3O_4 (111) are more stable (Yu et al. 2012). Therefore, Fe_3O_4 (111) was selected as the model surface. Among the six terminations of Fe_3O_4 (111), the surface with both Fe_{Oct} and Fe_{Tet} are stable and highly reactive. Therefore, a twelve-layer periodic slab model terminated with Fe_{Oct} and Fe_{Tet} was chosen as the research model, shown in Figure 1. The six bottom layers were fixed while the six outmost layers were fully relaxed.

Theoretical methods

Spin-polarized DFT calculations were performed by embedded DMol3 module in Materials Studio (MS) software (Delley 2000, 2010). In the calculation, the generalized gradient approximation (GGA) using the Perdew-Burke-Ernzerhof (PBE) functional with DFT-D correction was chosen to describe the exchange-correlation function (Perdew, Burke, and Ernzerhof 1996; Peverati and Baldridge 2008). The double-numerical basis with

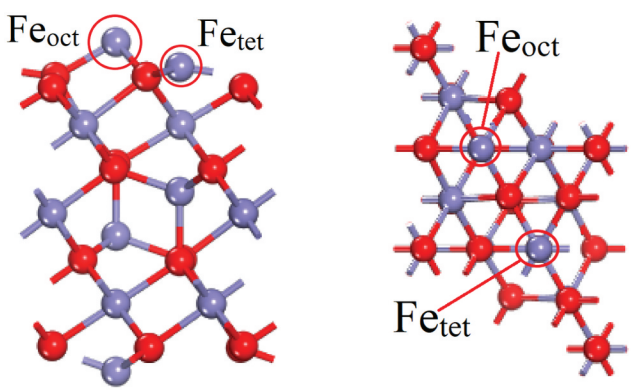

Figure 1. Optimized structures of Fe_3O_4 (111) from the top and side views. Bond distances are in Å. (Fe atoms are purple; O atoms are red.).

polarization functions (DNP) was adopted. The real-space global orbital cutoff radius was set as 4.8 Å. The Brillouin-zone was integrated with 4 × 4 x 4 and 4 × 4 x 1 *k*-point sampling using the Monkhorst-Pack method for bulk lattice and surface adsorption system. The convergence criteria for SCF (self-consistent field), energy, force and displacement were 1×10^{-6} Ha, 1×10^{-5} Ha, 0.002 Ha/Å and 0.005 Å, respectively. A vacuum layer of 20 Å was introduced to avoid the influence between two Fe_3O_4 (111) layers.

To describe the interaction between molecules and catalytic surface, the adsorption energy (E_{ads}) of relevant species was calculated by $E_{ads} = E_{S+gas}$ - E_S - E_{gas}, where E_{S+gas}, E_S, and E_{gas} represented the total energies of the adsorbed configuration, the Fe_3O_4 (111) surface, and the isolated species, respectively. E_{ads} is generally used to judge the chemisorption or physisorption form in theoretical chemistry field. A larger negative value of E_{ads} indicated more energetically favorable adsorption. Some studies (Wang 2007) believe that the E_{ads} range of physisorption is above −0.83 eV, while others (Nørskov, Studt, and Abild-Pedersen 2014) proposed that E_{ads} for physisorption ranges from −1.0 eV to −0.1 eV. In this study, the adsorption is defined as chemisorption when $E_{ads} < -0.83$ eV. The reaction pathways were explored via the search of transition state (TS), which was the transient product during the reaction (Vineyard 1957). In this work, TS was determined by using liner synchronous transit (LST)/quadratic synchronous transit (QST) (Halgren and Lipscomb 1977). The vibrational frequency calculation was performed on the obtained TS structure to ensure that only one imaginary frequency corresponding to the reaction coordinate existed.

The reaction rate constant (k) was further obtained based on the transition-state theory (TST) (Vineyard 1957). It is expressed as

$$k = \frac{k_B T}{h} exp\left(\frac{-\Delta G_a}{RT}\right) \tag{1}$$

where k_B is Boltzmann constant, T is temperature, h is Plank constant, G_a is Gibbs free energy difference between the transition state and the reactant state, and R is the universal gas constant. Gibbs free energy G is calculated by

$$G = H - TS \tag{2}$$

where G is composed of electronic energy, zero-point energy (ZPE) and the thermal contributions from vibration, rotation, and translation. Therefore, based on the ideal gas approximation, the enthalpy H is calculated by

$$H(T) = E^{elc} + \mathrm{ZPE} + E_{vib}(T) + E_{rot}(T) + E_{trans}(T) + RT \tag{3}$$

And entropy S is calculated by

$$S(T) = S_{vib}(T) + S_{rot}(T) + S_{trans}(T) \tag{4}$$

Results and discussion

Adsorption of NO and CO on Fe_3O_4 (111)

The surface sites (Fe_{Oct}, Fe_{Tet}, and bridge site) are all tested for the adsorption of NO/CO with N/C down or O down configurations. The stable adsorption configurations of single

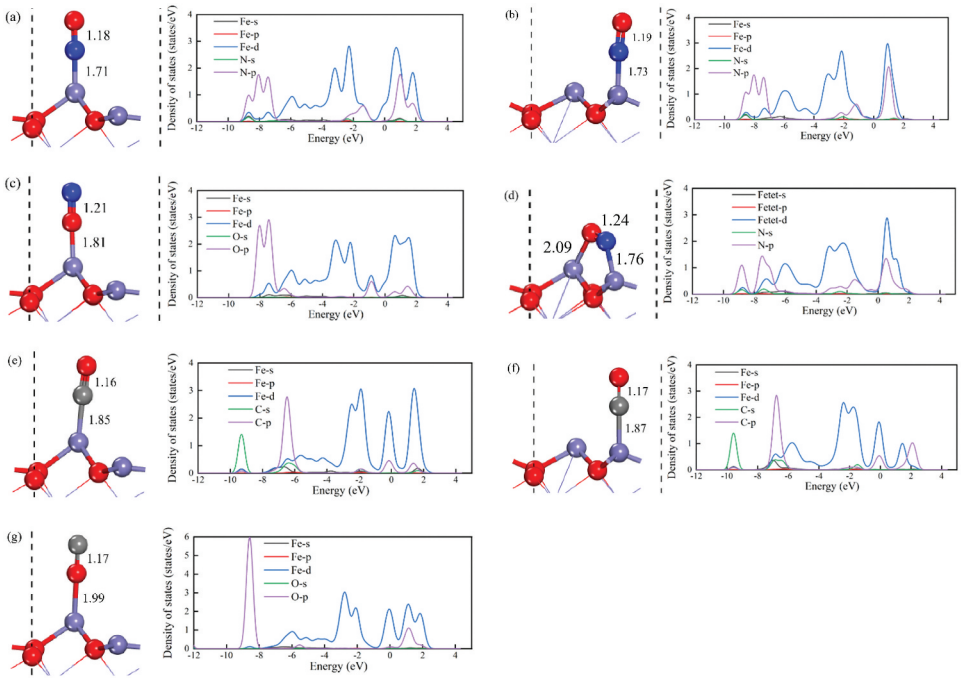

Figure 2. Optimized adsorption structures and PDOS of NO and CO: (a) *N*-down on Fe_{Oct}; (b) *N*-down on Fe_{Tet}; (c) O-down on Fe_{Oct}; (d) parallel(e) C-down on Fe_{Oct}; (f) C-down on Fe_{Tet}; (g) O-down on Fe_{Oct}; (h) two parallel NO; (i) two N-down NO; (j) two opposite NO; (k) two ringy NO. Bond distances are in Å. Fe atoms are purple, N atoms are blue, C atoms are gray and O atoms are red.

NO/CO on Fe_3O_4 (111) are displayed in Figure 2. It can be seen that NO molecule interacts with Fe atom on the surface through its N or O atom. The active sites can be Fe_{Oct} or Fe_{tet} for the *N*-down cases (Figures 2a,b), while the O-down NO only adsorbs on the Fe_{Oct} site (Figure 2c). It is found that when NO is first put near the Fe_{Tet} site as O-down configuration it will finally become the *N*-down configuration at Fe_{Oct} site. This indicates that Fe_{Oct} site has more intense interaction with NO than Fe_{Tet} site. Thus, the unstable O-down configuration tends to transform to stable *N*-down configuration at Fe_{Oct} without energy barrier. Besides, NO can be attached to the surface in parallel pattern (Figure 2d). To clarify the absorption type, E_{ads}'s, and bond length of these configurations were calculated and Mulliken analysis was performed. The results are given in Table 1. Clearly, the adsorption structures of single NO molecule all belong to chemisorption with N-down configuration

Table 1. Adsorption energies, bond length and Milliken analysis of different structures.

Gas	Structure	E_{ads} (eV)	$R_{Fe\text{-}N/O/C}$ (Å)	$R_{N/C\text{-}O}$ (Å)	Q (e)
NO	a	−2.66	1.71	1.18	0.126
	b	−1.81	1.73	1.19	0.225
	c	−1.38	1.81	1.21	0.230
	d	−2.04	2.09/1.76	1.24	0.369
CO	e	−1.72	1.85	1.16	0.092
	f	−0.86	1.87	1.17	0.189
	g	−0.30	1.99	1.17	0.125

having the largest absolute E_{ads} (−2.66 eV), also indicating Fe_{Oct} site is more active than Fe_{Tet} site. In addition, NO molecule obtains different electrons from the surface.

To further reveal the adsorption mechanism of NO on Fe_3O_4 (111), partial density of states (PDOS) of these structures were calculated. PDOS presents the energy contributions of each orbital of a given atom, and can be used to describe the electron hybridization in the system and thereby the formation of bonds. As presented in Figure 2a, the orbitals of Fe-s/p/d and *N*-s/p hybridize intensely near Fermi level at about −2.28 eV, −1.35 eV, 0.99 eV and 1.8 eV, indicating there is a strong chemisorption of NO on the surface. For the other structures displayed in Figures 2b–d, the hybridization mainly happens at −2.18/0.94 eV, −0.89/0.64/1.51 eV and −3.15/-2.29/0.60 eV, also proving the existence of the bond formation between NO and the surface and the chemisorption mechanism.

The results also show that when CO molecule approaches to Fe surface, it adheres on the surface perpendicularly either through C atom or O atom. Like NO, the unstable O-down configuration at Fe_{Tet} site will transform to stable C-down configuration at Fe_{Oct} site. Therefore, O-down adsorption of CO only happens on Fe_{Oct} site. The C-down structures have E_{ads} of −1.72 eV (Figure 2e) and −0.86 eV (Figure 2f), indicating both are chemisorption. However, E_{ads} for the O-down structures only has −0.30 eV, which is a typical value of physisorption. The smaller E_{ads} at Fe_{Oct} and the only O-down configuration at Fe_{Oct} site both illustrate Fe_{Oct} site is more active than Fe_{Tet} site. Besides, PDOS analysis shows that the hybridization of O-down CO and the surface mainly exists at the unoccupied states, confirming the corresponding process is a weak physisorption. Compared with NO, CO has smaller absolute E_{ads}, indicating that NO is more prone to adsorb on Fe_3O_4 (111) surface.

The adsorption of double NO molecules was also considered and the stable configurations are presented in Figure 3. Relevant structure parameters are summarized in Table 2. The values of E_{ads}'s are between −2.63 eV and −4.28 eV, ascribed to a strong chemisorption. To specify the interaction of two NO molecules when they are adsorbed on the surface, the energy difference ΔE was calculated by $\Delta E = E_{ads}(\text{NO-1}) + E_{ads}(\text{NO-2}) - E_{ads}(\text{2NO})$, where E_{ads}(NO-1) and E_{ads}(NO-2) represented E_{ads}'s of two corresponding single NO adsorption structures, and E_{ads}(2NO) represented E_{ads} of double NO molecules. The positive value of ΔE indicates that there exists interaction between two NO molecules on the surface.

As shown in Table 2, among these configurations, only ΔE of two ringy NO (Figure 3d) is positive. In this structure, two NO molecules can form a ringy structure, different with other configurations in which two NO molecules adsorb separately. This dimer structure, denoted as $(NO)_2$, is also found in many literatures (Esrafili 2018; Hu et al. 2020; Yan et al. 2021) and is usually regarded as an important reaction intermediate in NO reduction.

The direct dissociation of NO over iron oxide surface

As shown above, the adsorption of NO on Fe_3O_4 (111) surface is stronger than that of CO. When NO is adsorbed on surface, there are mainly two reaction pathways of NO reduction by CO: NO-dissociation and $(NO)_2$ dimer (Esrafili 2018). For the former one, NO on the surface dissociates into N and O atoms and then two N atoms recombine into a N_2 molecule. For the latter one, $(NO)_2$ dimer decomposes into an O atom and a N_2O molecule. Therefore, three most stable structures shown in Figure 2 as the initial reactants (IS2, IS2 and IS3) are used to analyze the most possible NO-dissociation pathway.

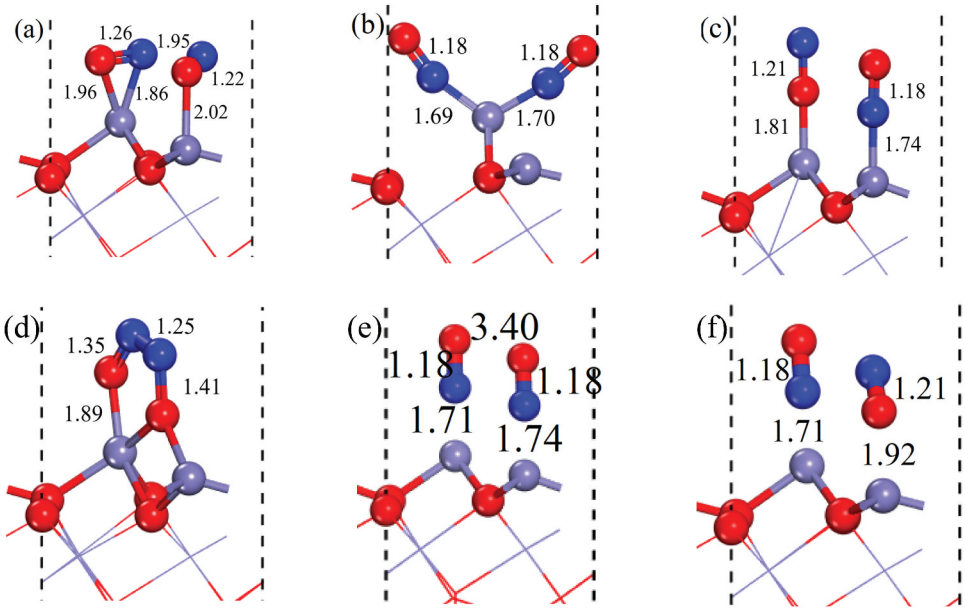

Figure 3. Optimized adsorption structures 2NO: (a) two parallel NO; (b) two *N*-down NO on one site; (c) two opposite NO-1; (d) two ringy NO; (e) two *N*-down NO on two sites; (f) two opposite NO-2. Bond distances are in Å. Fe atoms are purple, N atoms are blue, C atoms are gray and O atoms are red.

Table 2. Adsorption energies, bond length and energy difference of different 2NO structures.

Structures	E_{ads} (eV)	$R_{Fe\text{-}N/O/C}$ (Å)	$R_{N/C\text{-}O}$ (Å)	ΔE (eV)
a	−2.63	1.96/1.86/2.02	1.26/1.22	−0.79
b	−3.83	1.69/1.70	1.18/1.18	−1.49
c	−3.01	1.81/1.74	1.21/1/18	−0.18
d	−3.59	1.89/1.41	1.35/1.25	0.83
e	−4.28	1.71/1.74	1.18/1.18	−0.19
f	−3.29	1.71/1.92	1.18/1.21	−0.75

Shown in Figure 4, the absorbed NO molecule dissociates into N_{ads} and O_{ads} atoms through a transition state (TS1, TS2 and TS3) with high energy barriers (E_a = 3.10 eV, 2.36 eV and 2.12 eV). Compared with E_a's (0.63–5.38 eV) for different catalysts reported by literatures (Deushi, Ishikawa, and Nakai 2017; Esrafili 2018; Fajín, Cordeiro, and Gomes 2012; Mudchimo et al. 2018; Xie et al. 2012; Yan et al. 2021), E_a's over Fe_3O_4 (111) are relatively high. Besides, the dissociation reactions are endothermic. Therefore, NO-dissociation pathway is less favorable in both kinetics and thermodynamics.

Decomposition of $(NO)_2$ dimer over iron oxide surface

The potential energy profile of $(NO)_2$ dimer pathway is displayed in Figure 5. The $(NO)_2$ dimer structure forms on the surface as the initial state (IS4), and then one of the *N*-O bonds gradually increases from 1.41 Å to 1.90 Å in the transition state (TS4). At the same time, Fe-O bond elongates to 2.05 Å, leading to the generation of N_2O. The process only needs to

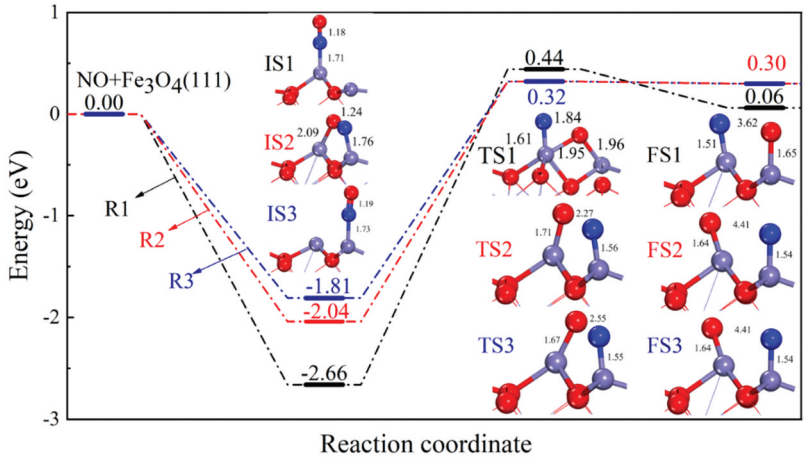

Figure 4. Possible reaction pathways of NO dissociation. Bond distances are in Å.

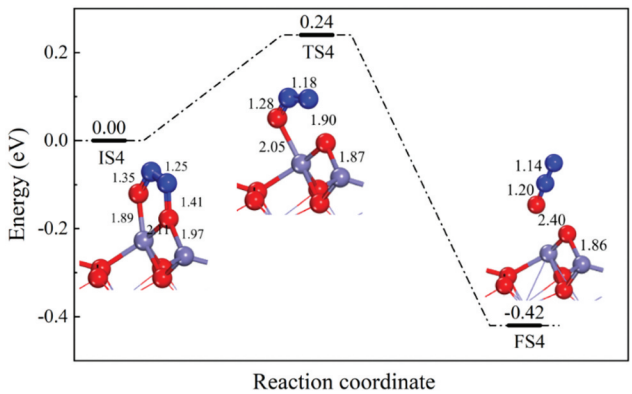

Figure 5. Possible reaction pathway for $(NO)_2$ dimer decomposition. Bond distances are in Å.

overcome an E_a of 0.24 eV. Moreover, the reaction is exothermic by 0.42 eV, which could provide the energy to activate the reactants in IS4. The comparisons of E_a on different catalysts and the method used in different references are listed in Table 3. The decomposition of $(NO)_2$ dimer can happen on different catalysts such as Si/Pd/Ni-doped boron nitride nanosheet and Au (321) surface as shown in Table 3. Although they may use different method, the results can still provide a reference for the evaluation of different catalysts. It can be seen E_a of Fe_3O_4 (111) is rather small compared with the results of 0.39–0.92 eV from the previous studies (Esrafili 2018; Esrafili, Heydari, and Dinparast 2019; Fajín, Cordeiro, and Gomes 2012; Hu et al. 2020), indicating that the process on Fe_3O_4(111) is kinetically favorable and easy to occur.

The generated N_2O could be decomposed through gas reaction or on the surface of Fe_3O_4. Figure 6 depicts the possible reaction pathway of decomposition of N_2O with and without CO in gas reaction. In absence of CO, N_2O molecule surpasses a rather high E_a (3.51 eV) to break into N_2 and an O atom. The result is consistent with the previous findings that N_2O dissociates at high temperatures (>1173 K) (Amrousse et al. 2013). However,

Table 3. Comparisons of E_a in different references.

Researcher	E_a (eV)	catalysts	Method (functional)
Hu et al. (2020)	0.24	Fe_3O_4 (111) surface	GGA/PBE
Esrafili (2018)	0.39	Si-doped boron nitride nanosheet	GGA/PBE
Fajín, Cordeiro, and Gomes (2012)	0.92	Au (321) surface	GGA/PAW
Esrafili, Heydari, and Dinparast (2019)	0.65/0.69	Pd/Ni-doped boron nitride nanosheet	M06-2X

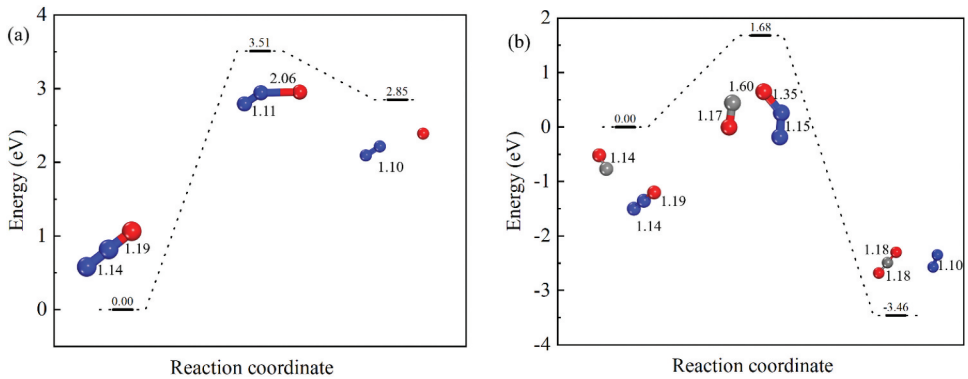

Figure 6. Possible reaction pathway for the dissociation of N_2O: (a) without CO; (b) with CO. Bond distances are in Å.

when CO is added, this E_a decreases to 1.68 eV, with CO_2 and N_2 generated. Therefore, CO can promote the decomposition of N_2O in the gas phase.

Besides, the generated N_2O from the decomposition of $(NO)_2$ dimer could reabsorb onto the surface. To assess the associated mechanism, DFT studies are conducted on two stable configurations by locating one N_2O molecule on the different sites of Fe_3O_4 (111) surface, as shown in Figure 7. When N_2O molecule approaches the surface with *N*-down, it can adsorb on the Fe_{Oct} site with an E_{ads} of −0.89 eV. The corresponding PDOS results show that bond exists between Fe and N atoms. The length of *N*-O bond (1.20 Å) remains almost unchanged compared with that of free N_2O molecule (1.19 Å). However, when N_2O attaches to the surface with O-down, it decomposes into an O atom and an N_2 molecule, adsorbing on Fe_{Oct} and Fe_{Tet} sites respectively. The E_{ads} of this configuration is as high as −2.35 eV, indicating a strong chemisorption. The PDOS results show that there exists intense hybridization between O-2*p* and Fe_{Oct}-3*d* orbitals, indicating a strong interaction between O atom and the surface. The interaction of N_2 with Fe_{Tet} is much weaker, meaning that N_2 molecule is easier to desorb from surface than O atom. The stable configuration of the remaining O_{ads} and its PDOS results are shown in Figure 7c. The O_{ads} atom has an E_{ads} as high as −5.42 eV. The large overlap of Fe-d orbital and O-d orbital further indicates there is strong interaction between O_{ads} and the surface. As a result, the stable O_{ads} will occupy the active sites of Fe_{Oct} and Fe_{Tet} and thus impede the decomposition of $(NO)_2$ dimer.

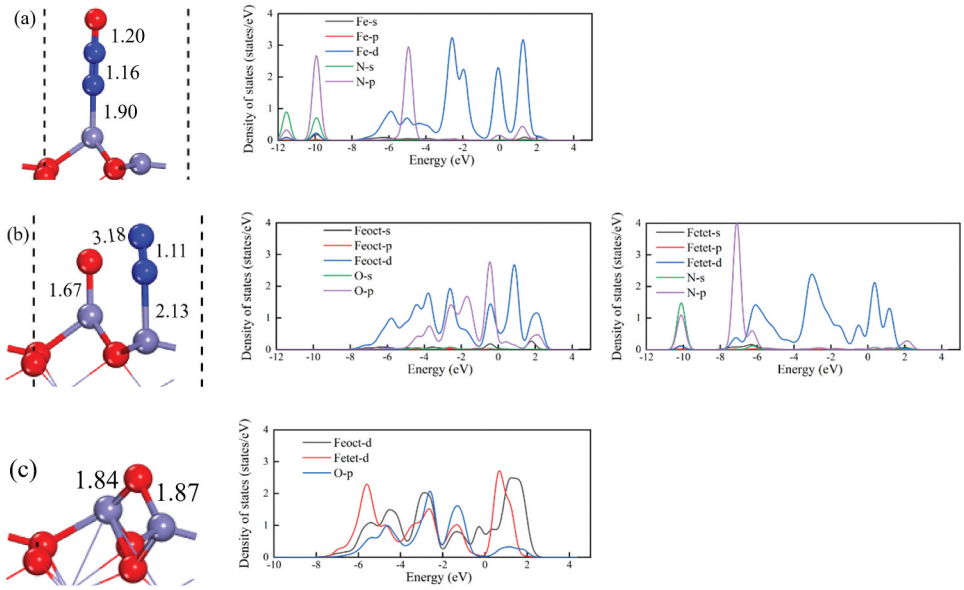

Figure 7. The adsorption configurations and PDOS results of N_2O on Fe_3O_4 (111): (a) *N*-down on Fe-Oct; (b) decomposition on both Fe-Oct and Fe-Tet. The adsorption of O atom on Fe_3O_4 (111) and its PDOS: (c). Bond distances are in Å.

The removal of O_{ads} atom in presence of CO

As a reductant, CO can promote the reduction of NO. The proceeding of the reaction depends on effective removal of the remaining O_{ads} species. Figure 8 shows the possible reaction pathways in presence of CO. It can be seen the free CO molecule can adsorb simultaneously with O_{ads} on Fe_{Oct} (IS6) or Fe_{Tet} (IS5) sites with C-down. Then C atom and O_{ads} in IS5 get closer from 2.82 Å to 1.95 Å (TS5). Meanwhile, the Fe-O_{ads} bond is weaken, with the bond length elongated to 2.25 Å. Finally, CO_2 molecule is produced (FS5). This process has a small E_a (0.14 eV) and is exothermic with 1.36 eV. The generated CO_2 has a moderate E_{ads} (−0.78 eV), indicating that CO_2 will be easy to desorb. IS6 reactant

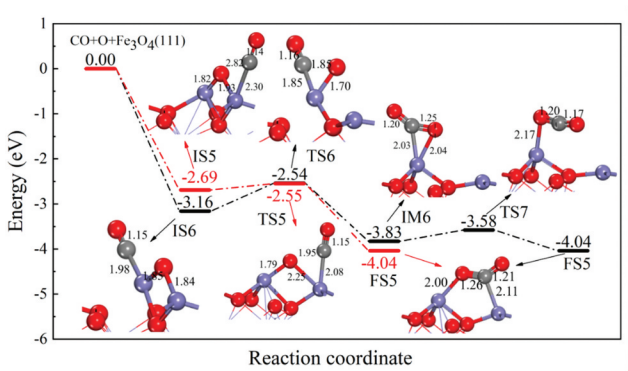

Figure 8. Possible reaction pathway for the removal of O_{ads} species. Bond distances are in Å.

overcomes an E_{ads} of 0.62 eV to produce TS6, and then obtains a CO_2 molecule adsorbed on Fe_{Oct} as an intermediate structure IM6. After that, IM6 may change into a relatively more stable configuration (FS5) with a small E_a of 0.25 eV. Therefore, through both pathways, O_{ads} will be easily removed with the presence of CO.

The effect of O_2

Previous studies show that NO reduction rate decreases severely in the presence of O_2 (Li et al. 2012). Therefore, the adsorption of O_2 on the surface is studied. As shown in Figure 9, E_{ads}'s of the two typical adsorption structures are −2.09 eV and −2.52 eV, respectively, which are comparable with that of NO. Therefore, O_2 has a competitive effect against NO and CO when they reach the surface of Fe_3O_4 (111). This could impede the reduction of NO by occupying the surface-active sites. Besides, previous researches also show that Fe-based catalysts could also catalyze the oxidation of CO by O_2 (Kim and Han 2017; Yang et al. 2017). Therefore, there could exist a competing reaction of CO with O_2 relevant to the reduction of NO by CO over Fe_3O_4 (111). In general, from both the view of gas adsorption and reaction, the inhibited effect of O_2 could be ascribed to the occupation of active sites and the oxidation of CO.

The reaction rate constants of different reactions

Figure 10 depicts the reaction rate constants k's of elementary reactions as discussed above at different temperatures. $k_{NOdis\text{-}1}$, $k_{NOdis\text{-}2}$ and $k_{NOdis\text{-}3}$ represent the k's of three NO dissociation reactions as displayed in Figure 4. $k_{CO+O\text{-}1}$ and $k_{CO+O\text{-}2}$ represent the k's of IS6→TS6→IM6 and IS5→TS5→FS5 as shown in Figure 8, respectively. $k_{(NO)2dis}$ is the k of decomposition of $(NO)_2$ dimer described in Figure 5. $k_{CO2des\text{-}1}$ and $k_{CO2des\text{-}2}$ designate the k's of CO_2 desorption from the surface. It can be found that all k's increase with increasing temperature, however, with different dependence degree. Even at a high temperature (1123 K), $k_{NOdis\text{-}1}$, $k_{NOdis\text{-}2}$ and $k_{NOdis\text{-}3}$ are still close to zero, indicating that NO is hard to decompose under this circumstance. However, the k's of other reactions are several orders of magnitude higher than that of NO dissociation, confirming the possible reaction pathways: $2NO \rightarrow (NO)_2^*$, $(NO)_2^* \rightarrow N_2O + O^*$, and $O^* + CO^* \rightarrow CO_2$. For all the elementary

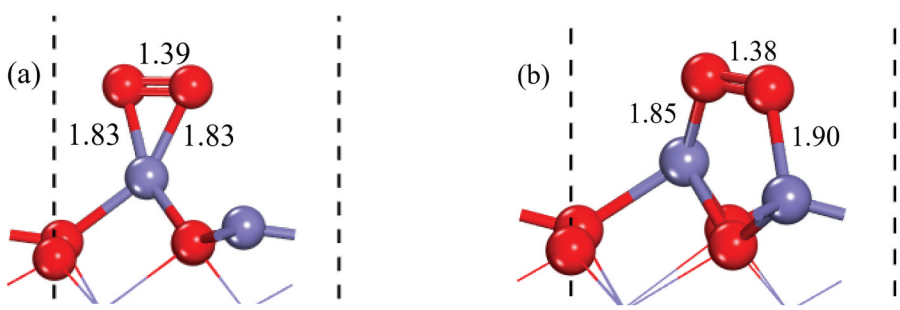

Figure 9. Adsorption structure of O_2 on Fe_3O_4(111): (a) O_2 on Fe_{Oct}; (b) O_2 on both Fe_{Oct} and Fe_{Tet}. Bond distances are in Å.

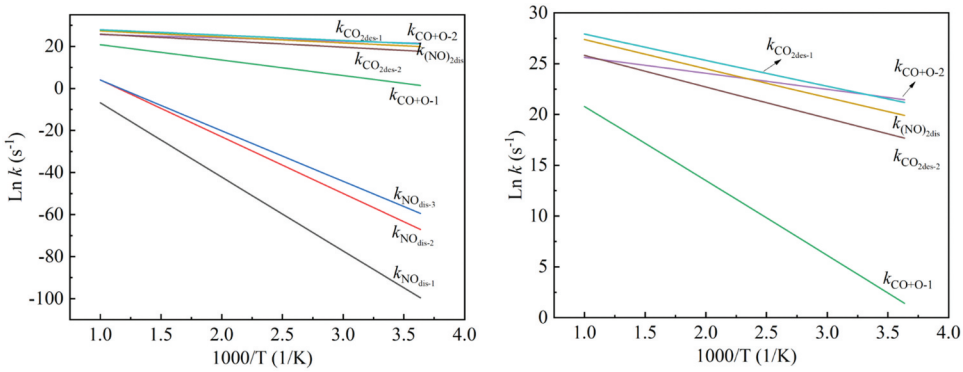

Figure 10. Reaction rate constants of elementary reactions at different temperatures.

reactions of this pathway, k_{CO+O-1} is obviously smaller than others under different temperatures. Therefore, the rate-limiting step is the removal of O atom from the surface.

Conclusions

The adsorption configurations of CO and NO on Fe_3O_4 and the reaction mechanisms are explored via DFT calculations. Results indicated that the tetrahedral and octahedral Fe sites (Fe_{Oct} and Fe_{Tet}) on Fe_3O_4 are the active sites for NO/CO's chemisorption adsorption. NO has higher adsorption energy than CO and it is difficult to dissociate once it absorbs on Fe_3O_4 surface because of the high energy barrier. In addition, $(NO)_2$ dimer mechanism is found to be a possible pathway for the reduction of NO by CO over Fe_3O_4, following three steps: $2NO \rightarrow (NO)_2^*$, $(NO)_2^* \rightarrow N_2O + O^*$, and $O^* + CO^* \rightarrow CO_2^*$. The $(NO)_2$ dimer structure formed by the adsorption can decompose via a small energy barrier into a N_2O molecule and an O atom adsorbing strongly on the surface, and then the surface O atom can be removed by CO. It was also found O_2 will prevent the NO reduction reaction. The calculated reaction rate constants further verify the existence of $(NO)_2$ dimer mechanism and the rate-limiting step is the removal of the surface O atom.

Acknowledgement

This work is supported by the National Key Development Project (2020YFB0606303) and National Natural Science Foundation of China (U1710251).

Disclosure statement

No potential conflict of interest was reported by the author(s).

Funding

The work was supported by the National Natural Science Foundation of China [U1710251]; National Key Development Project [2020YFB0606303]

References

Amrousse, R., A. Tsutsumi, A. Bachar, and D. Lahcene. 2013. N_2O catalytic decomposition over nano-sized particles of Co-substituted Fe_3O_4 substrates. *Appl. Catal A-Gen* 450:253–60. doi:10.1016/J.APCATA.2012.10.036.

Boningari, T., S. M. Pavani, P. R. Ettireddy, S. S. C. Chuang, and P. G. Smirniotis. 2018. Mechanistic investigations on NO reduction with CO over Mn/TiO_2 catalyst at low temperatures, Mol. *Catal* 451:33–42. doi:10.1016/j.mcat.2017.10.017.

Busch, M., V. Mehar, L. R. Merte, M. Shipilin, E. Lundgren, J. F. Weaver, and H. Grönbeck. 2018. Adsorption of NO on Fe_3O_4(111). *Chem. Phys. Lett* 693:84–87. doi:10.1016/j.cplett.2017.12.069.

Cheng, X. X., Y. R. Cheng, Z. Q. Wang, and C. Y. Ma. 2018. Comparative study of coal based catalysts for NO adsorption and NO reduction by CO. *Fuel* 214:230–41. doi:10.1016/j.fuel.2017.11.009.

Chen, H. S., Z. Zheng, Z. W. Chen, W. Z. Yu, and J. R. Yue. 2017. Multistep reduction kinetics of fine iron ore with carbon monoxide in a micro fluidized bed reaction analyzer, metall. Mater. *Trans. B* 48:841–52. doi:10.1007/s11663-016-0883-7.

Delley, B. 2000. From molecules to solids with the DMol3 approach. *J. Chem. Phys.* 113 (18):7756–64. doi:10.1063/1.1316015.

Delley, B. 2010. Time dependent density functional theory with DMol 3. *J. Phys. Condens. Mat* 22 (38):384208. doi:10.1088/0953-8984/22/38/384208.

Deushi, F., A. Ishikawa, and H. Nakai. 2017. Density functional theory analysis of elementary reactions in NOx reduction on Rh surfaces and Rh clusters. *J. Phys. Chem. C* 121 (28):15272–81. doi:10.1021/acs.jpcc.7b04526.

Esrafili, M. D. 2018. NO reduction by CO molecule over Si-doped boron nitride nanosheet: A dispersion-corrected DFT study. *Chem. Phys. Lett* 695:131–37. doi:10.1016/j.cplett.2018.02.020.

Esrafili, M. D., S. Heydari, and L. Dinparast. 2019. A comparative DFT study about surface reactivity and catalytic activity of Pd- and Ni-doped BN nanosheets: NO reduction by CO molecule. *Struct. Chem* 30 (5):1647–57. doi:10.1007/S11224-019-01355-4.

Fajín, J. L. C., M. N. D. S. Cordeiro, and J. R. B. Gomes. 2012. Unraveling the mechanism of the NO reduction by CO on gold based catalysts. *J. Catal* 289:11–20. doi:10.1016/j.jcat.2012.01.010.

Halgren, T. A., and W. N. Lipscomb. 1977. The synchronous-transit method for determining reaction pathways and locating molecular transition states. *Chem. Phys. Lett* 49 (2):225–32. doi:10.1016/0009-2614(77)80574-5.

Hayhurst, A. N., and A. D. Lawrence. 1997. The reduction of the nitrogen oxides NO and N_2O to molecular nitrogen in the presence of iron, its oxides, and carbon monoxide in a hot fluidized bed, Combust. *Flame* 110 (3):351–65. doi:10.1016/S0010-2180(97)00085-0.

Hayhurst, A. N., and Y. Ninomiyas. 1998. Kinetics of the conversion of NO to N_2 during the oxidation of iron particles by NO in a hot fluidised bed. *Chem. Eng. Sci* 53 (8):1481–89. doi:10.1016/S0009-2509(98)00009-8.

Hou, X. S., Z. Hai, Y. Shi, J. F. Lu, and G. X. Yue. 2008. N_2O decomposition over the circulating ashes from coal-fired CFB boilers. *Chem. Eng. J* 140 (1–3):43–51. doi:10.1016/j.cej.2007.08.033.

Hu, L. L., Y. Zhang, H. Zhang, and Y. Wu. 2020. Catalytic reduction of NO by CO over Fe-doped penta-graphene as a promising catalyst: A density functional study, Mol. *Catal* 496:111194. doi:10.1016/j.mcat.2020.111194.

Kim, K., and J. W. Han. 2017. Mechanistic study for enhanced CO oxidation activity on (Mn, Fe) Co-doped CeO_2(111. *Catal. Today* 293-294:82–88. doi:10.1016/j.cattod.2016.11.046.

Li, J., G. H. Luo, Y. Chu, and F. Wei. 2012. Experimental and modeling analysis of NO reduction by CO for a FCC regeneration process. *Chem. Eng. J* 184:168–75. doi:10.1016/j.cej.2012.01.024.

Li, J. J., Y. Zhang, H. R. Yang, and Y. M. Yang. 2016. Study of the effect of ash composition in coal on the kinetic parameters of NO reduction reaction by CO. *J. China Coal Society* 41:2448–53.

Monazam, E. R., R. W. Breault, and R. Siriwardane. 2014. Reduction of hematite (Fe_2O_3) to wüstite (FeO) by carbon monoxide (CO) for chemical looping combustion. *Chem. Eng. J* 242:204–10. doi:10.1016/j.cej.2013.12.040.

Mudchimo, T., S. Namuangruk, N. Kungwan, and S. Jungsuttiwong. 2018. Carbon-Doped boron nitride nanosheet as a promising metal-free catalyst for NO reduction: DFT mechanistic study. *Appl. Catal. A-Gen* 557:79–88. doi:10.1016/j.apcata.2018.02.025.

Nørskov, J. K., F. Studt, and F. Abild-Pedersen. 2014. *Fundamental concepts in heterogeneous catalysis*. Palo Alto: John Wiley & Sons.

Perdew, J. P., K. Burke, and M. Ernzerhof. 1996. Generalized gradient approximation made simple. *Phys. Rev. Lett.* 77 (18):3865. doi:10.1103/physrevlett.77.3865.

Peverati, R., and K. Baldridge. 2008. Implementation and performance of DFT-D with respect to basis set and functional for study of dispersion interactions in nanoscale aromatic hydrocarbons. *J. Chem. Theory Comput* 4 (12):2030–48. doi:10.1021/ct1002187.

Prabakaran, V., and S. Jayanti. 2019. Complete reduction of ilmenite by CO in chemical looping combustion—multistep kinetic model approach, Energ. *Fuel* 33 (7):6585–90. doi:10.1021/acs.energyfuels.9b01018.

Qin, Y. H., L. Huang, J. X. Zheng, and Q. Ren. 2016. Low-Temperature selective catalytic reduction of NO with CO over A-Cu-BTC and AOx/CuOy/C catalyst. *Inorg. Chem. Commun* 72:78–82. doi:10.1016/j.inoche.2016.08.018.

Sholl, D., and J. A. Steckel. 2009. *Density functional theory: A practical introduction*. Hoboken: Wiley. doi:10.1002/9780470447710.

Vineyard, G. H. 1957. Frequency factors and isotope effects in solid state rate processes. *J. Phys. Chem. Solids* 3 (1–2):121–27. doi:10.1016/0022-3697(57)90059-8.

Wang, S. L. 2007. *Physical chemistry*. Beijing: Metallurgy Industry Press.

Wang, Y. D., X. N. Hua, C. C. Zhao, T. T. Fu, W. Li, and W. Wang. 2017. Step-Wise reduction kinetics of Fe_2O_3 by CO/CO_2 mixtures for chemical looping hydrogen generation. *Int. J. Hydrogen Energ* 42 (9):5667–75. doi:10.1016/j.ijhydene.2017.01.159.

Wang, R., C. Zou, and Y. Zhang. 2022. A DFT study of N_2O homogeneous and heterogeneous reduction reaction by the carbon monoxide[j]. *Combust. Sci. Technol* 194 (5):963–76.

Wright, J. P., J. P. Attfield, and P. G. Radaelli. 2002. Charge ordered structure of magnetite Fe3O4 below the Verwey transition. *Phys. Rev. B* 66 (21):214422. doi:10.1103/PhysRevB.66.214422.

Xie, H. J., M. Ren, Q. F. Lei, W. J. Fang, and F. Ying. 2012. Explore the catalytic reaction mechanism in the reduction of NO by CO on the Rh^{7+}++ cluster: A quantum chemical study. *J. Phys. Chem. C* 116 (14):7776–81. doi:10.1021/jp2118357.

Xue, P., Z. Fu, X. Chu, Y. X. Zhang, and Z. X. Yang. 2014. Density functional theory study on the interaction of CO with the Fe3O4 (0 0 1) surface[j]. *Appl. Surf. Sci.* 317:752–59.

Xu, C. B., S. L. Wu, D. Q. Cang, Q. S. Shou, M. Li, and Y. Deng. 1999. The catalytic performance of several metallic oxides and complex metallic oxides on reaction of CO reducing NO. *Chin. J. Environ. Sci* 1:31–33.

Yang, T., R. Fukuda, S. Hosokawa, T. Tanaka, S. Sakaki, and M. Ehara. 2017. A theoretical investigation on CO oxidation by single-atom catalysts $M_1/\gamma\text{-}Al_2O_{3\ (M=pd,\ Fe,\ Co,\ and\ Ni)}$. *Chem. Cat. Chem* 9:1222–29. doi:10.1002/cctc.201601713.

Yan, X. C., J. Liu, Y. J. Yang, Z. Wang, and Y. Zheng. 2021. A catalytic reaction scheme for NO reduction by CO over Mn-terminated $LaMnO_3$ perovskite: A DFT study, fuel process. *Technol* 216:106798. doi:10.1016/j.fuproc.2021.106798.

Yue, T., K. Wang, C. Wang, Y. Tong, J. Gao, X. Zhang, P. Zuo, L. Tong, and Q. Liang. 2020. Emission characteristics of hazardous atmospheric pollutants from ultra-low emission coal-fired industrial boilers in China. *Aerosol Air Qual. Res* 20 (4):877–88. doi:10.4209/aaqr.2019.10.0531.

Yu, X. H., C. F. Huo, Y. W. Li, J. G. Wang, and H. J. Jiao. 2012. Fe_3O_4 surface electronic structures and stability from GGA+U, Surf. *Sci* 606:872–79. doi:10.1016/j.susc.2012.02.003.

Zhou, H. S., J. D. Lu, and H. Zhou. 2001. The reduction of nitrogen oxides N_2O/NO in the presence of Fe, its oxides, and CO in fluidized bed combustion of coal, Proceedings-Chinese Society of Electrical Engineering, Beijing, China 21: 44–47.

Zhou, C. S., H. M. Yang, D. X. Qi, J. X. Sun, J. M. Chen, Z. Y. Zhang, L. Mao, Z. J. Song, and L. S. Sun. 2018. Insights into the heterogeneous HgO oxidation mechanism by H_2O_2 over Fe_3O_4 (0 0 1) surface using periodic DFT method. *Fuel* 216:513–20. doi:10.1016/j.fuel.2017.12.004.